UCRL-83885
PREPRINT
CONF-791027--2

A Fokker-Planck/Transport Model for Neutral Beam Driven Tokamaks

John Killeen
Arthur A. Mirin
Michel G. McCoy

MASTER

This paper was prepared for the
Autumn College on Plasma Physics
International Centre for Theoretical Physics
Trieste, Italy
November, 1979

January, 1980

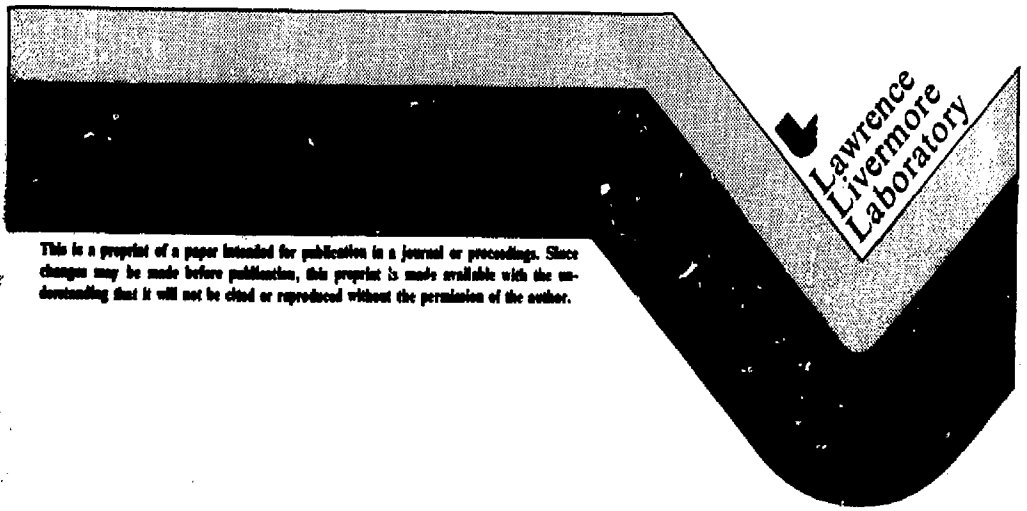

A FOKKER-PLANCK/TRANSPORT MODEL FOR NEUTRAL BEAM DRIVEN TOKAMAKS *

J. Killeen, A.A. Mirin, and M.G. McCoy
Magnetic Fusion Energy Computer Center
Lawrence Livermore Laboratory
Livermore, California, U.S.A.

Abstract

The application of non-linear Fokker-Planck models to the study of beam-driven plasmas is briefly reviewed. This evolution of models has led to a Fokker-Planck/Transport (FPT) model for neutral-beam-driven Tokamaks, which is described in detail. The FPT code has been applied to the PLT, PDX, and TFTR Tokamaks, and some representative results are presented.

1. INTRODUCTION

The need for a Fokker-Planck [1] description of a beam-driven plasma was recognized in the 1950's. An early proposal [2] for a two-energy component DT reactor discussed the non-Maxwellian character of such a plasma, and in particular described the "depletion" of low energy electrons caused by the presence of the hot ion component. This conjecture [3,4] was studied using a two species Fokker-Planck code [5], developed to calculate energy transfer from hot ions to cold electrons in a plasma [6].

Energy transfer between ions and electrons is usually calculated by using the Spitzer [7] formulae. These transfer rates are based on a quasi-equilibrium theory assuming that

---

*Work performed under the auspices of the U.S. Department of Energy by the Lawrence Livermore Laboratory under contract number W-7405-ENG-48.

the electrons have Maxwellian velocity distributions. It was conjectured [3,4] that the transfer rate would be less than the stated value in those cases where the ions are considerably hotter than the electrons. The ions exchange energy primarily with electrons whose velocities are lower than the mean ion velocity. Estimates were made [3,4] that the slow electrons would be scattered by ions to higher velocities faster than they would diffuse downward in velocity to fill this hole in the distribution. This depletion of the small velocity end of the electron distribution was observed in the Fokker-Planck calculations [6]. The consequence in these cases is that the transfer rates are less than the Spitzer values.

Fokker-Planck models are also needed for the study of beam-driven mirror confined plasmas [8], because of the presence of the loss cone in velocity space and the ambipolar potential. Killeen and Futch [9,10] and Fowler and Rankin [11,12] solved the Fokker-Planck equations for both ions and electrons, assuming that the evolution of the distribution functions could be described by the equations for isotropic distributions, with certain factors included to take the presence of the loss cone and ambipolar potential into account. The Fowler and Rankin code was for a steady-state model, whereas the Killeen and Futch code was time dependent and included the effects of charge exchange and time dependent build-up of a plasma formed by neutral injection.

A multispecies model [13,14] was developed in order to

study beam-driven DT and D^3He mirror reactors, including the effects of reaction products. The principal assumptions of this model are that the "Rosenbluth potentials" [1] are isotropic and that the distribution functions can be represented by their lowest angular eigenfunction. An extensive parameter study [14] was conducted, yielding values of the confinement parameter $n\tau$ and the figure of merit Q (the ratio of thermonuclear power to injected power) as a function of mirror ratio and injection energy.

The first injection of neutral beams into Tokamak plasmas took place at the Culham, Princeton, and Oak Ridge laboratories in 1972-73. The injected ions were studied with linearized Fokker-Planck models [15,16,17] and the expected plasma heating was observed experimentally.

With the advent of much more powerful neutral beams, it is now possible to consider neutral-beam-driven Tokamak fusion reactors. For such devices, three operating regimes [18] can be considered: (1) the beam-driven thermonuclear reactor, (2) the two-energy component torus (TCT), and (3) the energetic-ion-reactor e.g., the counterstreaming ion torus (CIT). In order to study reactors in regimes (2) or (3), a non-linear Fokker-Planck model must be used because most of the fusion energy is produced by beam-beam or beam-plasma reactions. Furthermore, when co and counter injection are used, or major radius compression is employed, a two velocity-space dimensional Fokker-Planck operator is required.

Fortunately, a non-linear, two-dimensional, multi-species

Fokker-Planck model [13,19] had been developed for the mirror program in 1973. This model was applied successfully to several scenarios of TCT operation [20,21,22].

An important element of these simulations is the calculation of the energy multiplication factor, Q, [19] for the various operating scenarios. This involves an accurate calculation of $\langle\sigma v\rangle$ for each pair of reacting species. The methods developed for computing these multi-dimensional integrals are reported elsewhere [23,24], and are briefly reviewed in Section 2.

The successful application of the two-dimensional Fokker-Planck model to the energy multiplication studies of TCT led to the formulation of a more complete model of beam-driven Tokamak behavior [25]. The Fokker-Planck /Transport (FPT) code in its present form is described in Section 2. The FPT code has been evolving since 1975 [22], and it has been applied to a CIT reactor study [26] and to the large Princeton Tokamaks [27-30]. Some representative results are presented in Section 3.

2. FOKKER-PLANCK/TRANSPORT MODEL

Neutral-beam-heated tokamaks are characterized by the presence of one or more energetic ion species which are quite non-Maxwellian, along with a warm Maxwellian bulk plasma. This background plasma may be described by a set of fluid equations. However, for scenarios in which there is a large energetic ion population, it is very important to represent the energetic species by means of velocity space distribution

functions and to follow their evolution in time by integrating the Fokker-Planck equations. It is essential to utilize the full nonlinear Fokker-Planck operator to assure that the slowing down and scattering of these energetic species are computed accurately and realistically.

The model presented here, in addition to solving one-dimensional radial transport equations for the bulk plasma densities and temperatures, solves nonlinear Fokker-Planck equations in two-dimensional velocity space for the energetic ion distribution functions. Moreover, neutral beam deposition and neutral transport are modeled using appended Monte Carlo codes developed elsewhere [31,32].

2.1 Energetic Ions

We consider an arbitary number of energetic ion species, whose presence derives from the ionization and charge exchange of injected fast neutrals. These species are described by distribution functions $f_b(v,\theta,r,t)$ in three-dimensional phase space, where b denotes the particle species, v is the velocity magnitude, θ is the pitch angle with respect to the magnetic field, and r is the distance from the magnetic axis. We assume that the flux surfaces are concentric circular torii.

2.1.1 Fokker-Planck Equations

The kinetic equation for the distribution function of energetic species b is

$$\frac{\partial f_b}{\partial t} = \left(\frac{\partial f_b}{\partial t}\right)_c + H_b - S_{bc} + S_{bcx} + \left(\frac{\partial f_b}{\partial t}\right)_E + \left(\frac{\partial f_b}{\partial t}\right)_r - L_b^{\alpha} - L_b^{orb} \quad . \tag{2.1}$$

The collision term $\left(\frac{\partial f_b}{\partial t}\right)_c$ is given by the complete nonlinear Fokker-Planck operator as derived by Rosenbluth, et al. [1].

It may be expressed in the form

$$\left(\frac{\partial f_b}{\partial t}\right)_c = \frac{1}{v^2}\frac{\partial}{\partial v}\left(A_b f_b + B_b \frac{\partial f_b}{\partial v} + C_b \frac{\partial f_b}{\partial \theta}\right) + \frac{1}{v^2 \sin\theta}\cdot\frac{\partial}{\partial \theta}\left(D_b f_b + E_b \frac{\partial f_b}{\partial v} + F_b \frac{\partial f_b}{\partial \theta}\right) , \tag{2.2}$$

where the coefficients A_b through F_b are sums of moments of the distribution functions of all charged species present [13,19]. The quantity H_b is the source resulting from the injection of neutral species b. S_{bc} represents the deceleration of energetic ions into the bulk plasma. S_{bcx} represents charge exchange between ion species b and the various neutral species. The quantity $\left(\frac{\partial f_b}{\partial t}\right)_E$ models the effect of the toroidal electric field. The term $\left(\frac{\partial f_b}{\partial t}\right)_r$ represents radial diffusion of the energetic ions. L_b^{α} is a fusion depletion term, and L_b^{orb} represents orbit losses. These terms are thoroughly described in the following two sections.

The numerical solution of this type of equation has been extensively studied [13,19]. In the FPT code, a new, fast,

vectorized program package [33] is utilized. We employ either implicit operator splitting or the Peaceman Rachford Alternating Direction Implicit (ADI) method [34].

It is not actually necessary to solve for distribution functions f_b on every flux surface where the bulk plasma ions are defined. Treating the energetic ions in detail on every fifth flux surface combined with cubic splines of velocity-space-integrated quantities yields accurate answers in a good deal less computer time.

2.1.2 Neutral Beam Deposition

The energetic ion source term H_b is calculated using the FREYA neutral beam deposition code [31]. This is a Monte Carlo code which takes into account the geometry of the tokamak and the precise locations and optical properties of the neutral beam injectors. A pseudo-collision technique is employed, i.e., particle penetration is based on the minimum mean free path throughout the plasma, and resulting collisions are analyzed, a posteriori, to see if they were genuine or false. This pseudo-collision technique enables one to compute potential collision points without calculating the intersection of the neutral path with each flux surface.

For use in the Fokker-Planck/Transport Code, several improvements have been made to FREYA:

a) A multispecies background is allowed. That is, the neutral mean free path is based on charge exchange and impact ionization with an arbitrary number of ion species (in

addition to electron impact ionization). The ionization and charge exchange cross-sections are taken from Ref. [35].

b) The reaction rate $\langle\sigma v\rangle$ for charge exchange and ion impact ionization is computed by averaging the product of the cross-section σ and the relative velocity over the ion distribution function. A 2D table look-up procedure is used.

c) All collisions with multiply charged ions are treated as ionizations, and only one charge state of any given impurity is considered. The total reaction rate between a neutral and an impurity ion of charge Z is taken as the equivalent proton rate times $Z^{1.35}$ [36].

d) When a neutral beam atom undergoes a charge-exchange, its location and energy are stored for later use in the neutral transport module, enabling the modeling of multiple charge exchanges and/or re-ionization.

e) The initial orbit of each deposited ion is analyzed. If that orbit strikes the limiter, the ion is discarded. This calculation assumes conservation of the toroidal component of the canonical angular momentum [37].

It is not necessary to call FREYA each timestep, as the neutral beam deposition term is usually slowly changing.

2.1.3 Other Source and Loss Terms

Energetic Ion Transfer. Each energetic ion species "b" has a corresponding background plasma component. As an energetic ion decelerates, if it is not lost, it will eventually join the bulk plasma. This process is simulated by transferring all "hot" ions below a specified energy from the

energetic ion distribution function to the corresponding bulk plasma component. This loss term, denoted S_{bc}, satisfies

$$\frac{m}{2}\int S_{bc}(v,\theta,r)\, v^2\, \underline{dv} \Big/ \int S_{bc}(v,\theta,r)\, \underline{dv} = \frac{3}{2} T_e(r) , \qquad (2.3)$$

where T_e is the electron temperature.

Charge-Exchange. The charge-exchange term is of the form

$$S_{bcx} = -f_b \sum_c \tilde{n}_c \langle \sigma v \rangle_{cx}^{cb} , \qquad (2.4)$$

where c runs over all neutral species (including neutral beam atoms) and $\tilde{n}_c$ is the corresponding neutral density. The charge exchange rate is taken from Ref. [36]. As can be seen, the charge exchange probability is assumed to be independent of ion energy.

Toroidal Electric Field. The acceleration by the electric field in the toroidal direction is given by

$$\left(\frac{\partial f_b}{\partial t}\right)_E = -a_{//} \frac{\partial f}{\partial v_{//}} = -\frac{Z_b e E_{//}}{m_b}\left(\cos\theta \frac{\partial f_b}{\partial v} - \frac{\sin\theta}{v}\frac{\partial f_b}{\partial \theta}\right) . \qquad (2.5)$$

Radial Diffusion. In a neutral-beam-heated plasma, the fast ions will have a velocity only two to three times greater than that of the bulk ions. Thus, it is reasonable to expect that the fast ions are subject to a certain amount of radial diffusion. We approximate this by the term

$$\left(\frac{\partial f_b}{\partial t}\right)_r = -\frac{f_b}{n_b} \cdot \frac{1}{r}\frac{\partial}{\partial r}\left(r D_b \frac{\partial n_b}{\partial r}\right) \quad , \tag{2.6}$$

where n_b is the hot ion density and D_b is a diffusion coefficient. This operator diffuses density but preserves velocity-space shape.

Fusion Depletion. For D-T plasmas a fusion loss term is included:

$$L_D^\alpha = \hat{n}_T \langle\sigma v\rangle_{DT} f_D$$
$$L_T^\alpha = \hat{n}_D \langle\sigma v\rangle_{DT} f_T \quad . \tag{2.7}$$

Here, $\hat{n}_D$ and $\hat{n}_T$ represent the total (bulk + hot) deuteron and triton densities, and the fusion rate, which is based on a cross-section given in detail in Ref. [14], is taken to be independent of energy.

Orbit Losses. Orbits through the various meshpoints (v,θ,r) are analyzed. This is complicated by the fact that whether or not an orbit intersects the limiter depends on the poloidal angle. We assume that the energetic ions are distributed uniformly with respect to poloidal angle, and we throw out an appropriate number, based on the fraction of orbits which do intersect the limiter.

2.2 Bulk Plasma Ions and Electrons

We consider an arbitrary number of bulk plasma ion species which are assumed to be Maxwellian in velocity space. These species are described by densities $n_a(r,t)$ and by a common temperature profile $T_i(r,t)$. The electrons have a

separately computed temperature profile $T_e(r,t)$, and their density is determined by quasineutrality; that is,

$$n_e = \sum_{\substack{\text{bulk}\\ \text{plasma}}} Z_a n_a + \sum_{\substack{\text{energetic}\\ \text{ions}}} Z_b n_b \quad . \tag{2.8}$$

2.2.1 Transport Equations

The ion densities and the ion and electron temperatures are described by the following set of equations:

$$\frac{\partial n_a}{\partial t} = -\frac{1}{r}\frac{\partial}{\partial r}\left(r\Gamma_a\right) + \int S_{bc}\,\underline{dv}\,\delta_{ab} + S_{ai} + S_{acx} - L_a^{\alpha} \tag{2.9}$$

$$\frac{\partial}{\partial t}\left(\frac{3}{2}\sum_a n_a T_i\right) = -\frac{1}{r}\frac{\partial}{\partial r}\left(r\sum_a Q_a\right) + \sum_{a,b}\int S_{bc}E_{bc}\,\underline{dv}\,\delta_{ab} + \sum_a S_{ai}\tilde{E}_a + W_{cx} - \frac{3}{2}T_i\sum_a L_a^{\alpha} + \sum_{a,b} Q_{ab} + Q_{\Delta} + \sum_a Q_{a\alpha} \tag{2.10}$$

$$\frac{\partial}{\partial t}\left(\frac{3}{2}n_e T_e\right) = -\frac{1}{r}\frac{\partial}{\partial r}\left(rQ_e\right) + Q_{eb} - Q_{\Delta} + Q_{e\alpha} - \frac{3}{2}\frac{n_e T_e}{\tau_r} + j_{\phi}E_{\phi} \quad . \tag{2.11}$$

The quantities Γ_a , Q_a and Q_e are particle and energy fluxes; E_{bc} is the mean energy of decelerated energetic ions; S_{ai} is the ionization source and $\tilde{E}_a$ is the energy of neutral species "a"; S_{acx} and W_{cx} describe charge exchange; L_a^{α} represents fusion depletion; Q_{ab} models heating by the energetic species; Q_{Δ} is energy exchange between bulk ions and electrons; $Q_{a\alpha}$ is alpha particle heating; τ_r is the radiation loss time; and $j_\phi E_\phi$ represents Ohmic heating.

2.2.2 Transport Models

The particle and energy fluxes are written as linear combinations of the density and temperature gradients and of the toroidal electric field. This makes possible the representation of a full multispecies neoclassical transport model, as described in Ref. [25]. However, present-day tokamaks do not seem to obey neoclassical scaling laws [38]; hence, the following transport model is employed.

We write the particle flux Γ_a as

$$\Gamma_a = -D_a \frac{\partial n_a}{\partial r} + R_a E_\phi \quad , \tag{2.12}$$

where

$$D_a = D_{0a} + D_{1a} r^3 + D_{2a}/n_e + D_{3a} n_e \tag{2.13}$$

and

$$R_a = 2.48c\left(\frac{r}{R}\right)^{1/2} \frac{n_a}{B_\theta} \quad . \tag{2.14}$$

The first term represents anomalous transport and the second term the effects of the Ware pinch.

The energy fluxes are written in terms of their convective and conductive components:

$$Q_a = \frac{5}{2} \Gamma_a T_i + K_{ia} n_a \frac{\partial T_i}{\partial r} \tag{2.15}$$

$$Q_e = \frac{5}{2} \Gamma_e T_e + K_e n_e \frac{\partial T_e}{\partial r} \quad , \tag{2.16}$$

where

$$\Gamma_e = \Sigma Z_a \left(D_a \frac{\partial n_a}{\partial r} - 0.8 R_a E_\phi \right) . \tag{2.17}$$

For the ion thermal conductivity we employ the neoclassical formula of Connor [39]:

$$K_{ia} = \frac{1.66 c^2 (r/R)^{1/2} T_i}{e^2 B_\theta^2} \frac{m_a}{Z_a^2} \cdot \left[\langle x_a^2 \nu_a \rangle - \langle x_a \nu_a \rangle^2 / \langle \nu_a \rangle \right] , \tag{2.18}$$

where the quantity in brackets is defined in Ref. [39]. For the electron thermal conductivity we use an empirical formula

$$K_e = K_{e0}/n_e + K_{e1}/n_e T_e \quad . \tag{2.19}$$

The current density j_ϕ is specified (usually parabolic to the three halves power), and the toroidal electric field E_ϕ is related to the current density through

$$E_\phi = \eta_s j_\phi \quad , \tag{2.20}$$

where η_s is the Spitzer resistivity [7].

2.2.3 Charge Exchange

The charge-exchange source for species "a" is expressed as

$$S_{acx} = \tilde{n}_a \sum_d n_d \langle\sigma v\rangle_{cx}^{ad} - n_a \sum_c \tilde{n}_c \langle\sigma v\rangle_{cx}^{ca} \quad . \tag{2.21}$$

Here, the first sum runs over all charged species (including energetic ones) and the second sum runs over all neutral species (including neutral beam atoms). The term $\tilde{n}_c$ represents the density of neutral species "c", and $\langle\sigma v\rangle_{cx}^{ca}$ is the charge-exchange rate between neutral species "c" and ion species "a".

The energy gained by the bulk ions due to charge exchange is

$$W_{cx} = \sum_{d,a} \tilde{n}_a n_d \langle\sigma v\rangle_{cx}^{ad} \tilde{E}_a - \sum_{c,a} \tilde{n}_c n_a \langle\sigma v\rangle_{cx}^{ca} \cdot \frac{3}{2} T_i \quad , \tag{2.22}$$

where "a" runs over all singly charged bulk plasma ions, "c" runs over all neutral species (including beam neutrals), and "d" runs over all ions (including energetic ions). Recall that any charge exchange between a neutral and a multiply charged ion is treated as an ionization.

2.2.4 Ionization

The ionization source for species "a" is

$$S_{ai} = \tilde{n}_a \left(n_e \langle\sigma v\rangle_{ie} + \sum_{\text{ions}} n_b \langle\sigma v\rangle_{ib} \right) \quad , \tag{2.23}$$

where electron and ion impact ionization are taken into account. As just noted, charge-exchanges with multiply charged ions are included in the second term. The ionization rate formulas are based on Ref. [35].

The ionization energy source is merely equal to $\sum_a S_{ai} \tilde{E}_a$, where $\tilde{E}_a$ is the energy of neutral species "a". There is a drawback in the model, in that energetic neutrals upon ionization become part of the bulk plasma. Energy is conserved, but momentum is not. The fact that this energetic tail is assumed to Maxwellianize instantly no doubt distorts the energy transfer with electrons.

2.2.5 Radiation

We consider only impurity radiation. The radiation loss time is written as

$$\tau_r = \frac{3}{2} T_e / \sum_Z n_Z L_Z \quad , \tag{2.24}$$

where the sum is over all impurity species. The cooling rate L_Z is expressed implicitly as

$$\log_{10} L_Z = \sum_{i=0}^{5} A_i \left(\log_{10} T_e\right)^i \quad , \tag{2.25}$$

where the coefficients A_i are enumerated in Ref. [40]. An arbitrary number of impurity species may be considered.

2.2.6 Energy Transfer

The energy transfer rate between bulk ions and electrons is

$$Q_{\Delta} = \sum_a \frac{3}{2} n_a (T_e - T_i)/\tau_{ea} \quad , \tag{2.26}$$

where τ_{ea} is the Spitzer energy-exchange time [7]. The above sum runs over all bulk plasma ions.

The heating of plasma ions and electrons by energetic ions is obtained from integrating the appropriate part of the Fokker-Planck collision operator. This results in the formula

$$Q_{ab} \sim \int_0^\infty f_a(v)v^2dv \cdot \left[\int_v^\infty f_b(x)xdx - \frac{m_a}{m_b}\frac{1}{v}\int_0^v f_b(x)x^2dx\right] \quad , \tag{2.27}$$

where "a" represents the plasma species, "b" is the energetic species, and $f_{a,b}$ are the respective distribution functions.

Alpha particle heating is computed in a similar manner.

2.2.7 Miscellaneous Terms

Fusion Depletion. For D-T plasmas a fusion loss term is included:

$$\begin{aligned} L_D^\alpha &= n_D \hat{n}_T \langle\sigma v\rangle_{DT} \\ L_T^\alpha &= n_T \hat{n}_D \langle\sigma v\rangle_{DT} \quad . \end{aligned} \tag{2.28}$$

Here the symbols n_D and n_T stand for the densities of the bulk deuterons and tritons, whereas the "hatted" symbols $\hat{n}_D$ and $\hat{n}_T$ include both bulk plasma and energetic ion contributions. The fusion rate is taken to be independent of energy.

Energetic Ion Transfer. The δ_{ab} appearing in Eq. (2.9) is a symbolic way of stating that plasma species "a" and energetic species "b" must really be the same species (e.g. both deuterons) for the transfer term to take effect. The quantity E_{bc} in Eq. (2.10) is the energy at which particles are transferred; in most cases, $E_{bc}=3/2T_e$.

2.2.8 Discretization of the Transport Equations

Eq's. (2.9)-(2.11) may be cast in the form

$$\frac{\partial \underline{u}}{\partial t} = \mathcal{L}(\underline{u}) \quad , \tag{2.29}$$

where the vector $\underline{u}$ consists of the bulk ion densities and the ion and electron energy-densities. An implicit, iterative difference scheme is employed; that is, we approximate Eq. (2.29) by

$$\frac{\underline{u}^{n+1} - \underline{u}^{n}}{\Delta t} = \rho \mathcal{L}_d(\underline{u}^{n+1}) + (1-\rho)\mathcal{L}_d(\underline{u}^{n}) \quad , \tag{2.30}$$

where Δt is the time increment, $\underline{u}^{n} = \underline{u}(t=n\Delta t)$, $0 \leq \rho \leq 1$, and the spatially discretized quantity $\mathcal{L}_d(\underline{u}^{n+1})$, which approximates $\mathcal{L}(\underline{u}^{n+1})$, is linearized with coefficients depending on the latest iterate. In particular, products of derivatives are written as

$$\left(\frac{\partial f}{\partial r}\frac{\partial g}{\partial r}\right)^{n+1} \approx \frac{1}{2}\left[\left(\hat{\frac{\partial f}{\partial r}}\right)^{n+1}\left(\hat{\frac{\partial g}{\partial r}}\right)^{*} + \left(\hat{\frac{\partial f}{\partial r}}\right)^{*}\left(\hat{\frac{\partial g}{\partial r}}\right)^{n+1}\right] \quad , \tag{2.31}$$

where * refers to the latest iterate and $\hat{}$ denotes a central difference approximation. Products of a function and a derivative are written as

$$\left(f\frac{\partial g}{\partial r}\right)^{n+1} \approx f^{*}\left(\hat{\frac{\partial}{\partial r}}\right)^{n+1} \quad , \tag{2.32}$$

and products of functions are written as

$$(fg)^{n+1} = \frac{1}{2}\left[f^{n+1}g^{*} + f^{*}g^{n+1}\right] \quad . \tag{2.33}$$

Second derivatives are approximated as

$$\left[\frac{\partial}{\partial r}\left(D\,\frac{\partial h}{\partial r}\right)\right]_j \simeq \left[\left(D\,\frac{\partial h}{\partial r}\right)_{j+1/2} - \left(D\,\frac{\partial h}{\partial r}\right)_{j-1/2}\right]\Big/\Delta r \quad , \tag{2.34}$$

with

$$\left(D\,\frac{\partial h}{\partial r}\right)_{j+1/2} = \left(\frac{D_j+D_{j+1}}{2}\right)\left(\frac{h_{j+1}-h_j}{\Delta r}\right) \quad , \tag{2.35}$$

where the subscript j indexes the radial variable.

An exception: The ion heat convection term $\frac{5}{2}\,\Gamma_a\,T_i$ uses the latest iterate for Γ_a and treats T_i implicitly, even though Γ_a contains derivatives. That is (dropping subscripts) for $\Gamma < 0$,

$$\frac{\partial}{\partial r}(\Gamma T) \simeq \frac{\Gamma_{j+1/2}\,T_j - \Gamma_{j-1/2}\,T_{j-1}}{\Delta r} \quad . \tag{2.36}$$

This linearization is appropriate for present-day transport models, in which ion heat convection dominates ion heat conduction--a fact which necessitates both implicit treatment of T_i and upwind differencing (as opposed to central differencing) of the heat convection term [41].

The boundary conditions are rather straight-forward. At the limiter, we impose small values of n_a, T_e and T_i. At r=0 we employ conservation boundary conditions. That is, Eq's. (2.9-2.11) are used but with flux derivatives $-\frac{1}{r}\frac{\partial}{\partial r}(rF)$ replaced by $-2F/_r$ evaluated one-half meshpoint in from the center. With the proper numerical integration scheme, the total number of ions and the total ion and electron energies

are properly conserved (modulo known source and loss terms). The resulting system of difference equations is block tridiagonal, and it is solved using standard methodology [34].

2.3 Neutrals

We consider an arbitrary number of monatomic neutral species, described by densities $\tilde{n}_a(r,t)$ and mean energies $\tilde{E}_a(r,t)$. These neutrals result from (1) charge-exchange of injected beam neutrals, (2) gas puffing, and (3) recycling from the limiter and wall. Neutral transport is computed using the AURORA code of Hughes and Post [32]. Although AURORA is a three-dimensional Monte Carlo code, it does not take into account toroidal effects, but instead assumes a long, straight cylinder. This of course results in some inaccuracies in the treatment of energetic neutrals. AURORA does not use a pseudo-collision technique. The local mean free path and distance travelled per zone must be computed for each particle. It is the time-consuming nature of this latter computation which necessitates the assumption of a cylindrical geometry rather than a toroidal one.

As is the case with FREYA, several improvements have been made in AURORA. It is now a multispecies neutrals transport code. An arbitrary number of charge exchanges involving an arbitrary number of species may be considered. The reaction rates $\langle\sigma v\rangle$ are computed as in FREYA, and all collisions with multiply charged ions are treated as ionizations. In addition, neutrals can be launched from any radius, thereby enabling consideration of neutrals arising from charge

exchange of injected beam neutrals. The neutral density profiles computed by AURORA are scaled to yield the correct integrated ionization rate. Also, neutral transport need not be computed every timestep, as that procedure would be too time-consuming.

2.4 Fusion

There are three contributions to the fusion reaction rate: (i) thermonuclear reactions, denoted R_{11}; (ii) "beam-target" reactions, denoted R_{12}; and (iii) reactions among the energetic ions, denoted R_{22}. At each plasma radius, the fusion reactivities $\langle\sigma v\rangle_{11}$, $\langle\sigma v\rangle_{12}$ and $\langle\sigma v\rangle_{22}$ are evaluated numerically via a five-fold velocity-space integral [23,24]:

$$R_{ij} = \int f_i(\underline{v}_i)\, f_j(\underline{v}_j)\, \sigma\, (\underline{v}_i - \underline{v}_j) |\underline{v}_i - \underline{v}_j| \underline{dv}_i \underline{dv}_j \quad . \tag{2.37}$$

The R_{ij} are then integrated over the plasma volume, to give the total reaction rate.

2.4.1 Deuteron Plasmas

In Deuteron plasmas two types of fusion reactions occur:

$$\begin{aligned} D + D &= T + p + 4.04 \text{ MeV} \\ D + D &= {}^3He + n + 3.27 \text{ MeV}. \end{aligned} \tag{2.38}$$

Each reaction probability is computed separately based on cross-sections found in Ref. [14]. We are thus able to monitor both the neutron production rate and the total fusion power. Because these reactions occur at such a slow rate, it is not necessary to include fusion depletion terms nor is it necessary to consider the effects of reaction products.

2.4.2 Deuteron-Triton Plasmas

Here it is necessary to consider only the reaction

$$D + T = \alpha + n + 17.58\ MeV \quad , \tag{2.39}$$

as the number of D-D reactions will be orders of magnitude smaller. The fusion cross-section may be found in Ref. [14]. Unlike the D-D case, the effects of the resulting fusion products (namely alpha particles) must be considered.

The alpha particle velocity distribution is taken to be the angle-averaged distribution given in Ref. [18]. Alpha heating is computed through integration of the Fokker-Planck collision operator. For computational convenience, all heat destined to be transferred from the alphas to the energetic ions is added to the bulk plasma ions instead. The alpha particle density is reduced in order to take into account the fact that some of the alpha particles will be lost on their first bounce. For this purpose we employ the subroutine of Shumaker [37]. Depletion of deuterons and tritons as a result of fusion is also modeled. This treatment of $f_\alpha(v)$ is reasonable only when plasma temperatures are changing slowly.

3. APPLICATIONS

The Fokker-Planck/Transport Code has been applied to several neutral-beam-injected tokamaks, including the Princeton Large Torus (PLT), the Poloidal Divertor Experiment (PDX), the Tokamak Fusion Test Reactor (TFTR) and the Divertor Injection Tokamak Experiment (DITE) [27-30,42]. We briefly highlight principal results of our applications to PLT and TFTR.

3.1 Applications to PLT

The Princeton Large Torus (PLT) has achieved record-setting temperatures. At high beam powers (e.g. 2.3 MW) and low plasma densities (e.g. $n_e(0) = 5.5 \times 10^{13}$ cm^{-3}), ion temperatures as high as 5.5 keV are reported [43]. Moreover, the fractional hot ion density on axis is measured to be up to 30 percent, and theoretical analyses indicate that at low density, the majority of the fusion neutrons result from either beam-beam or beam-target reactions [30].

Realizing that the energetic ions play a very important role and that it is crucial to model their time-evolution as realistically as possible, we proceed to analyze PLT with the FPT Code. A brief summary of PLT parameters is given in Table I.

3.1.1 Steady-State Calculations

The first set of calculations is designed to evaluate the treatment of the energetic ions. Using experimentally measured profiles of the electron density n_e, the electron temperature T_e, the toroidal electric field and the impurity content Z-effective (Z-effective$= 1/n_e \sum_{ions} Z_a^2 n_a$, and is taken to be independent of radius and due only to carbon), and using estimates of the ion temperature and neutral density profiles, the Fokker-Planck equations for the energetic ions are iterated to steady state. (The bulk plasma ion density is continually adjusted to maintain the prescribed electron density and impurity content.) The computed neutron fluxes

are then compared with the experimentally measured values. This comparison is carried out at peak neutron production, when the experiment itself has reached a quasi-steady-state. Results are shown in Figure 1.

We see that there is excellent agreement between code and experiment over a wide range of beam power (Ø.3 to 2 3 MW) and plasma density (The line-averaged electron density $\bar{n}_e$, which defined as $1/a\int_0^a n_e(r)dr$, where "a" is the plasma minor radius, ranges from 1.5 to 6.2×10^{13} cm^{-3}.). The principal uncertainties include (1) the ion temperature and neutral density profiles, (2) the fact that the experiment is not at an absolute steady state, (3) identification of the impurity, (4) calibration, and (5) the fact that only a limited number of experimental results are used.

3.1.2 Time-Dependent Calculations

Having established that the FPT code realistically models the energetic ions, we now consider time dependent modeling of the beam-injection phase of the experiment. For this purpose we make direct comparisons with August 1978 PLT shots.

At time Ø (the time when the beams are turned on), the density profile is assumed to vary as $(1-r^2/a^2)^3$. Carbon and iron impurities are chosen with $n_{iron} \equiv Ø.1 \cdot n_{carbon}$ and Z-effective constant in radius. The line averaged electron density $\bar{n}_e$ is matched to the experimentally measured value. The electron temperature and bulk ion temperature profiles also vary as parabolic cubed, and the initial temperature

values on axis $T_e(0)$ and $T_i(0)$ are estimated. The energetic ion density is of course assumed to be initially zero.

The code is then run for 150 ms, which is the approximate duration of beam injection. The amount of gas puffing is dynamically determined to match the experimentally measured electron line density $\bar{n}_e$. The impurity density profiles are adjusted to maintain a constant Z-effective, and a recycling coefficient R_c of 0.9 is prescribed. (The recycling coefficient R_c is defined as the neutral influx at the limiter divided by the ion outflux.)

We take as our primary transport model $D=5\times10^{16}/n_e$, $K_e=2.4\times10^{17}/n_eT_e$, K_i neoclassical and include the effects of the Ware Pinch, where the electron density n_e is in units of cm^{-3} and the electron temperature T_e is in keV. The code results at t = 150 ms are then compared with the experimental measurements.

Figures 2 and 3 compare the computed neutron fluxes with the experimentally measured values over a wide range of injection power and electron line density, respectively. Agreement to within a factor of 1.5 is obtained. The computed electron temperatures on axis are significantly lower than the experimental values, as can be seen in Figure 4. This suggests that errors in the electron transport are being balanced by errors elsewhere in the model, to yield the correct neutron flux.

We next investigate the effect of varying the transport model. Detailed comparisons of the electron density and

temperature profiles for PLT run number 88214 are shown in Figures 5 and 6. The computed density tends to be higher close to the axis and lower away from the axis, almost independent of transport model. Remember that the area under each density curve is the same, since the gas puffing rate has been dynamically chosen to match the experimentally measured $\bar{n}_e$. For all of the transport models considered, the computed T_e is lower than the experimentally measured value, and the experimental profile is more peaked on axis than any of the computed profiles. The shape and magnitude of the electron temperature varies considerably as the electron thermal conductivity K_e is varied. Comparisons with other experimental shots indicate that this trend is not uncommon. Thus, it is difficult to cite a particular transport model as being truly optimal.

3.2 Applications to TFTR

The Tokamak Fusion Test Reactor, which is currently under construction, is expected to come on line sometime in the early 1980's. It is hoped that this machine will achieve breakeven--that is, that the power produced from D-T fusion reactions will exceed the power of the injected neutral beams. In fact, proposals are under consideration to enhance the injection capability so that the ratio of output power to input power (denoted as Q) exceeds 2.

Several aspects of TFTR operation have been examined using the FPT code. Since this work has been presented in

detail elsewhere [29], we will briefly summarize our investigation and its principal results.

We first compare the perpendicular injection of 120 keV D^0 beams into a tritium bulk plasma fueled by recycling and gas puffing with the co- and counter-injection of 100 keV D^0 and 150 keV T^0 beams, respectively, into a plasma with a very low recycling coefficient. At small beam powers, the injection of D^0 and T^0 neutral beams is advantageous because the higher temperature and increased energetic ion fusion reaction rate outweigh the lower density. However at large beam powers, the larger density with D^0 on T combined with a reduced electron thermal conductivity and an increased alpha particle heating rate counteract the energy sink introduced by the cold puffed gas and recycled neutrals, thereby resulting in a substantially higher fusion rate.

We also examine the effects of varying the bulk ion diffusion coefficient, the energetic ion diffusion coefficient, the ion thermal conductivity and the recycling coefficient. We find that Q is highly dependent on the particle transport, thereby making it essential that definitive information from present experiments on the magnitude of the particle diffusion coefficient at high temperature be obtained.

4. CONCLUSIONS

We have described in detail a Fokker-Planck/Transport Code which is applicable to tokamaks in which there is intense

neutral beam injection. For such scenarios, where there is a large energetic ion population, it is essential to represent these energetic species by velocity space distribution functions and to follow their evolution in time by integrating nonlinear Fokker-Planck equations.

We have performed simulations of two large tokamaks--the Princeton Large Torus (PLT) and the Tokamak Fusion Test Reactor. Since the PLT is an active experiment, we have had the opportunity to make direct comparisons with the experimental results. We find that the computed neutron fluxes and the experimentally measured values agree to within 50 percent over a wide range of beam power and plasma density. For the TFTR we have compared two modes of operation--the injection of D^0 beams coupled with tritium gas puffing, and the injection of both D^0 and T^0 neutral beams. We see that TFTR performance depends strongly on injection power, plasma density (which is a function of the recycling coefficient and gas puffing rate), mode of injection, and the assumed transport model.

REFERENCES

1. M.N. Rosenbluth, et al., Phys. Rev. 107, 1 (1957).
2. W.I. Linlor, Hughes Aircraft Report No. 128 (1959).
3. W.I. Linlor, Bull. Am. Phys. Soc. II 4, 351 (1959).
4. C.B. Shaw, Bull. Am. Phys. Soc. II 5, 311 (1960).
5. J. Killeen and W. Heckrotte, Bull. Am. Phys. Soc. II 5, 311 (1960).
6. J. Killeen, et al., Nuclear Fusion Sup. Part 1, 183 (1962).
7. L. Spitzer, "Physics of Fully Ionized Gases" (Interscience, New York) 1956, 79.
8. J. Killeen and K.D. Marx, Methods in Comp. Phys. (Academic Press, New York), 9, 421 (1970).
9. J. Killeen and A.H. Futch, J. Comp. Phys., 2, 236 (1968).
10. A.H. Futch, et al., Phys. Fluids, 14, 1542 (1971).
11. T.K. Fowler and M. Rankin, Plasma Physics, 4, 311 (1962).
12. T.K. Fowler and M. Rankin, Plasma Physics, 8, 121 (1966).
13. J. Killeen and A.A. Mirin, Theoretical and Computational Plasma Physics, (IAEA, Vienna) 27, (1978).
14. A.H. Futch, et al., Plasma Physics, 14, 211 (1972).
15. J.G. Cordey and W.G.F. Core, Phys. Fluids, 17, 1626 (1974).
16. J.D. Gaffey, J. Plasma Physics, 16, 149 (1976).
17. J.D. Callen, et al., Plasma Physics and Controlled Nuclear Fusion Research (IAEA, Vienna) I, 645 (1975).
18. D.L. Jassby, Nuclear Fusion, 17, 309 (1977).
19. J. Killeen, et al., Methods in Comp. Physics (Academic Press, New York) 16, 389 (1976).

20. J. Killeen, et al., Lawrence Livermore Laboratory Report UCID-16530 (1974).

21. H.L. Berk, et al., Plasma Physics and Controlled Nuclear Fusion Research, (IAEA, Vienna) III, 569 (1974).

22. J. Killeen, et al., 7th European Conference on Controlled Fusion and Plasma Physics, 1, 22, (1975).

23. K.D. Marx, et al., Nuclear Fusion, 16, 702 (1976).

24. J.G. Cordey, et al., J. Comp. Phys., 28, 115 (1978).

25. A.A. Mirin, et al., J. Comp. Phys. 23, 23 (1977).

26. D.L. Jassby, et al., Plasma Physics and Controlled Nuclear Fusion Research, (IAEA, Vienna) II, 435 (1977).

27. D.E. Post, et al., Plasma Physics and Controlled Nuclear Fusion Research, (IAEA, Vienna) I, 471 (1978).

28. A.A. Mirin, et al., Heating in Toroidal Plasmas, (Grenoble, France) I, 13 (1978).

29. A.A. Mirin and D.L. Jassby, Lawrence Livermore Laboratory Report UCRL-81483, Rev. 1 (1979), also submitted to Nucl. Fusion.

30. P.L. Colestock, et al., Princeton Plasma Physics Laboratory Report No. PPPL-TM 325, (1979).

31. G.G. Lister, et al., Plasma Heating in Torodial Devices, (Varenna, Italy) 303 (1976).

32. M.H. Hughes and D.E. Post, J. Comp. Phys., 28, 43 (1978).

33. M.G. McCoy, A.A. Mirin, and J. Killeen, Lawrence Livermore Laboratory Report UCRL-83206 (1979).

34. R.D. Richtmyer and K.W. Morton, Difference Methods for Initial-Value Problems, (Interscience, New York), Second Edition (1967).

35. R.L. Freeman and E.M. Jones, Culham Laboratory Report CLM-R137 (1974).

36. R.E. Olson and A. Salop, Physical Review A, 16, 531 (1977).

37. D.E. Shumaker, private communication (1979).

38. H.P. Furth, Nucl. Fusion, 15, 487 (1975).

39. J.W. Connor, Plasma Physics, 15, 765 (1973).

40. D.E. Post, et al., Atomic Data and Nuclear Tables, 20, 397 (1977).

41. P.J. Roache, Computational Fluid Dynamics, (Hermosa, Albuquerque) 161, (1972).

42. R.D. Gill, et al., Ninth Euro. Conf. on Controlled Fusion and Plasma Physics (Oxford, UK) 150, (1979).

43. H. Eubank, et al., Plasma Physics and Controlled Nuclear Fusion Research, (IAEA, Vienna) I, 167, (1978).

Table I

REFERENCE PLT PARAMETERS

Major radius	1.40 m
Minor radius	0.40 m
$B_{toroidal}$	3.2 T
Plasma current	~0.5 MA
Neutral beam energy	~35 keV
Neutral beam power	Up to 3 MW 85% full energy 15% half energy
Injection angles	0°, 180°

Figure Captions

Fig. 1 Computed neutron fluxes vs. experimentally measured values for steady state PLT calculations.

Fig. 2 Ratio of computed to experimental neutron flux vs. injection power for transient PLT calculations.

Fig. 3 Ratio of computed to experimental neutron flux vs. electron line density for transient PLT calculations.

Fig. 4 Computed T_e vs. experimentally measured values for transient PLT calculations.

Fig. 5 Electron density profile vs. transport model for PLT run number 88214.

Fig. 6 Electron temperature profile vs. transport model for PLT run number 88214.

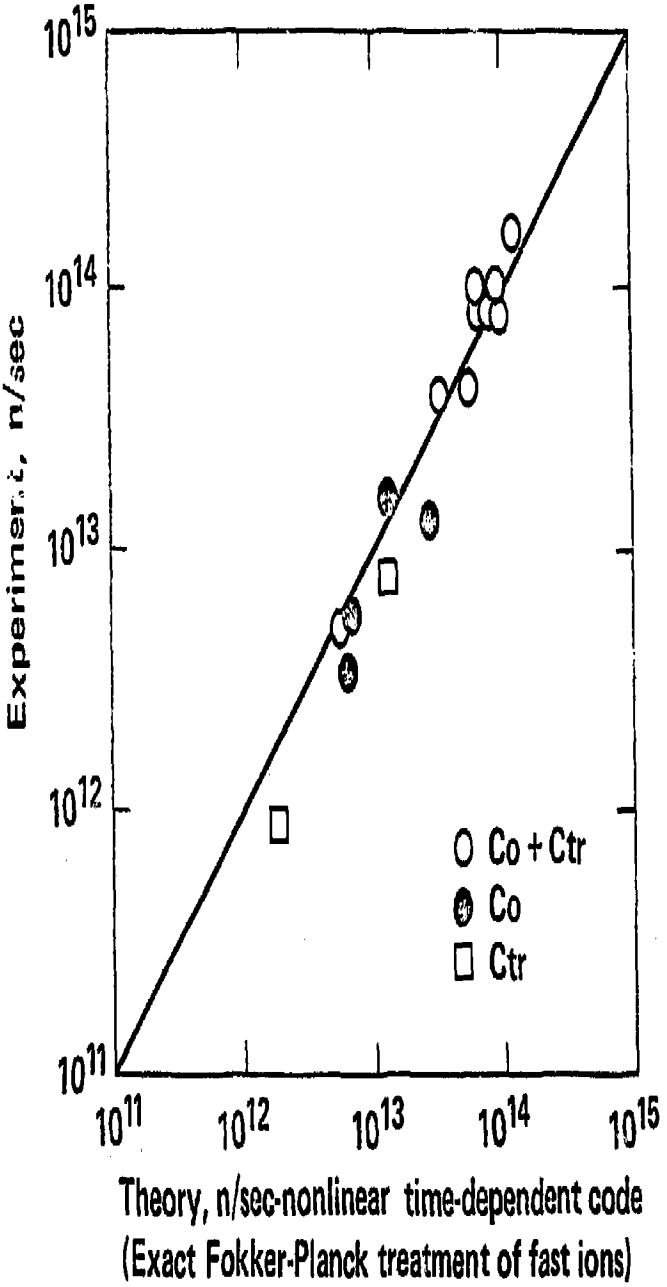

Fig. 1 Computed neutron fluxes vs. experimentally measured values for steady state PLT calculations.

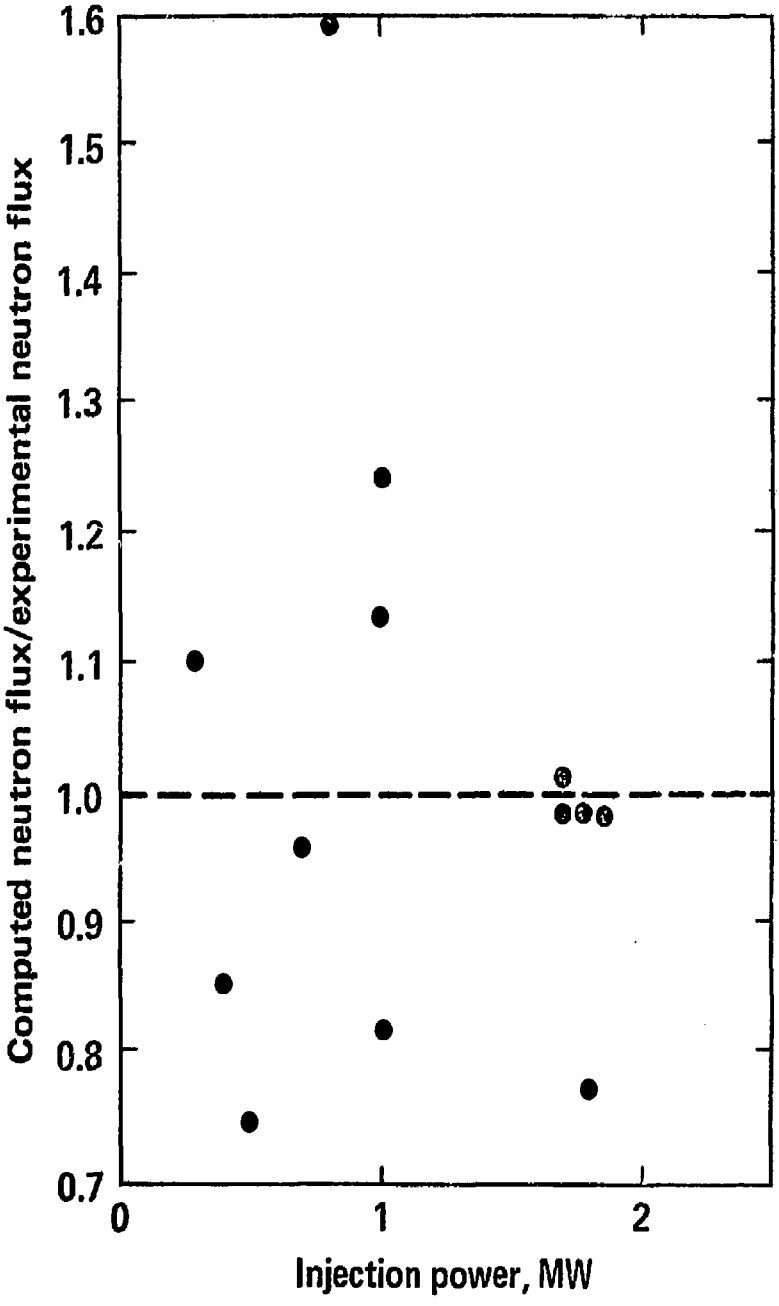

Fig. 2 Ratio of computed to experimental neutron flux vs. injection power for transient PLT calculations.

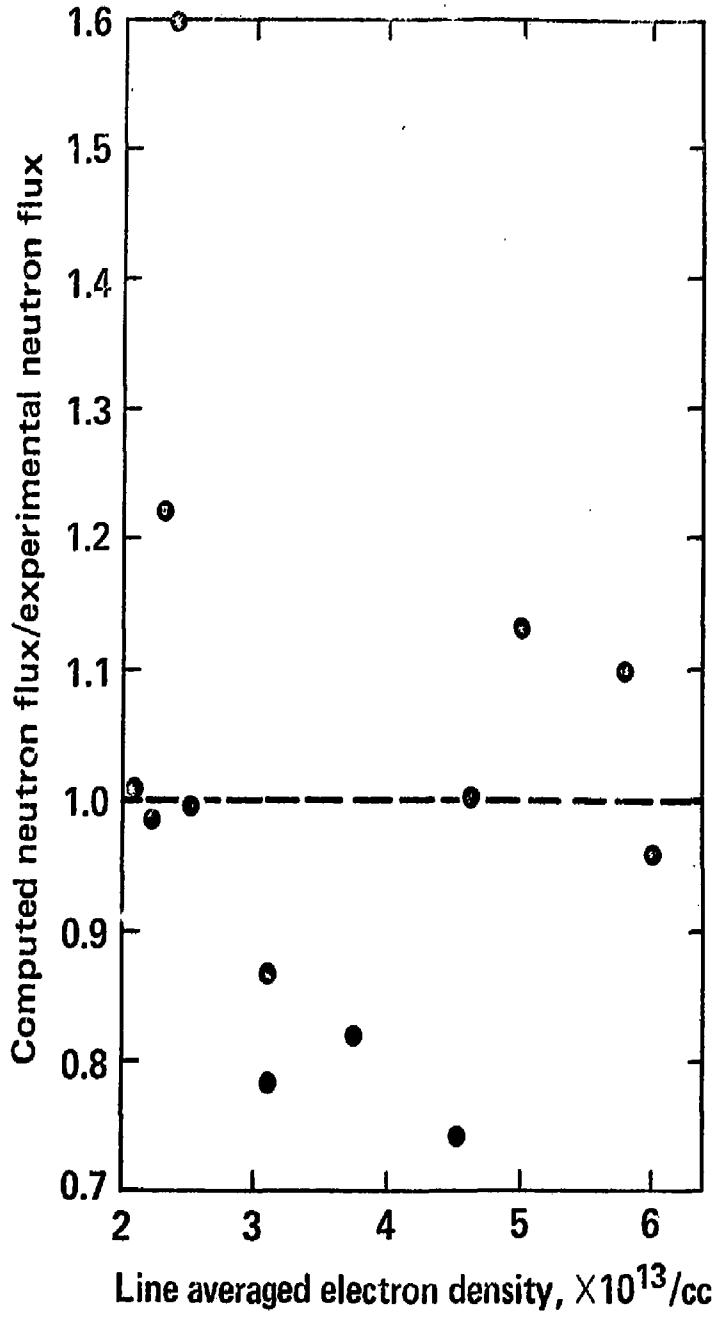

Fig. 3 Ratio of computed to experimental neutron flux vs. electron line density for transient PLT calculations.

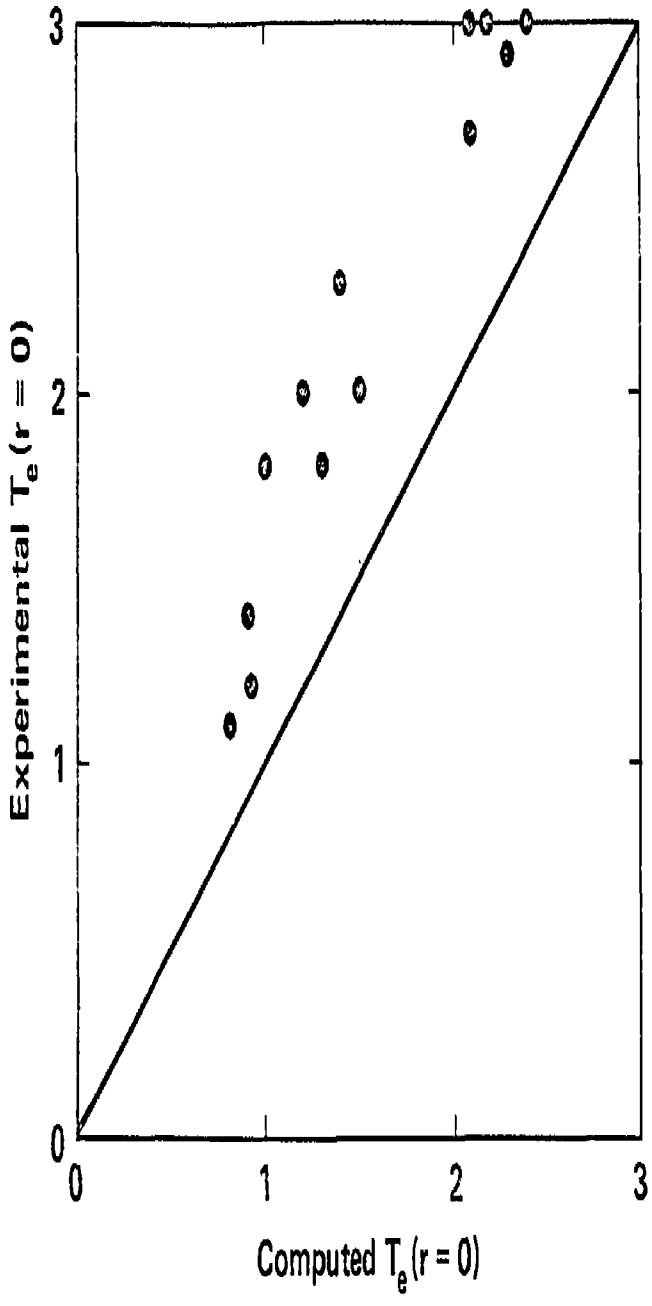

Fig. 4 Computed T_e vs. experimentally measured values for transient PLT calculations.

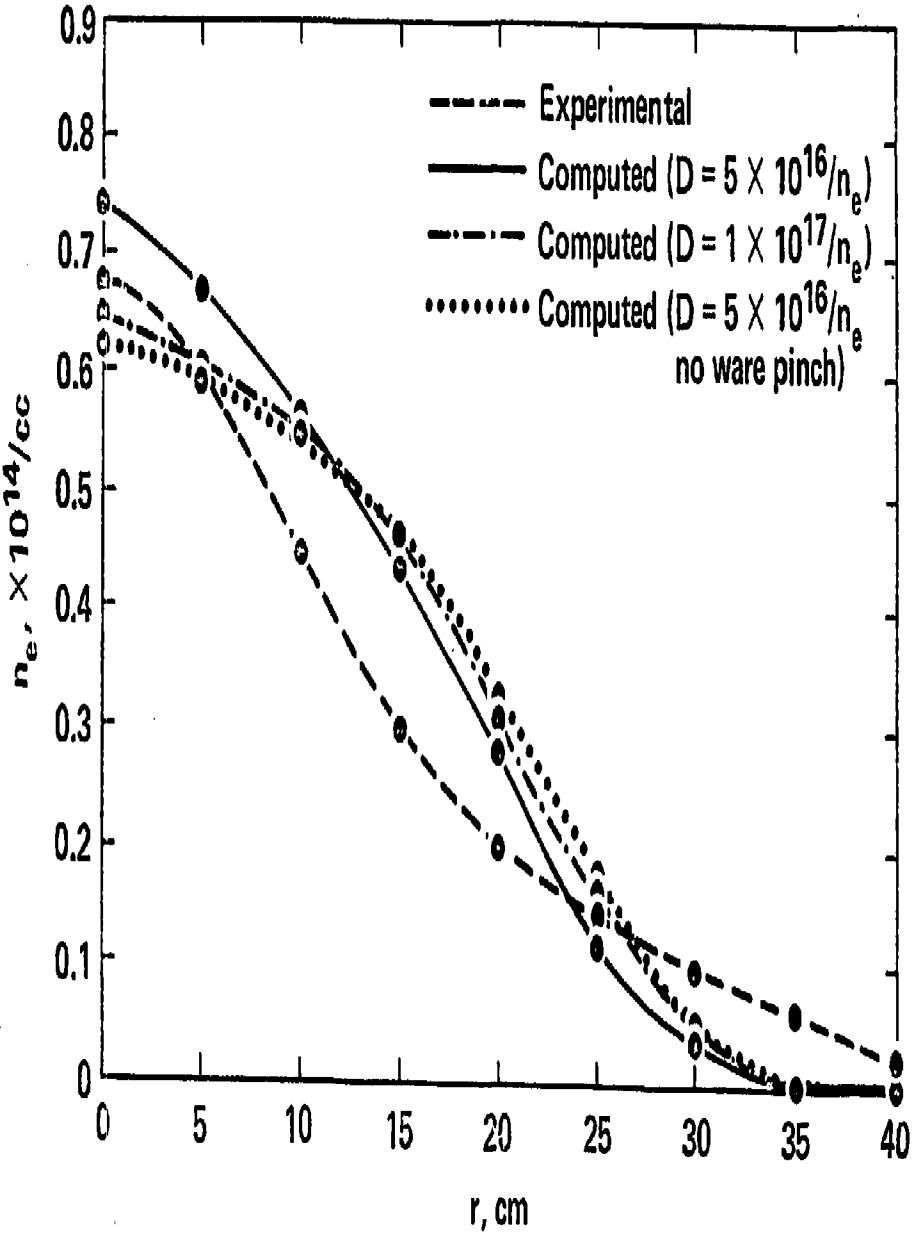

Fig. 5 Electron density profile vs. transport model for PLT run number 88214.

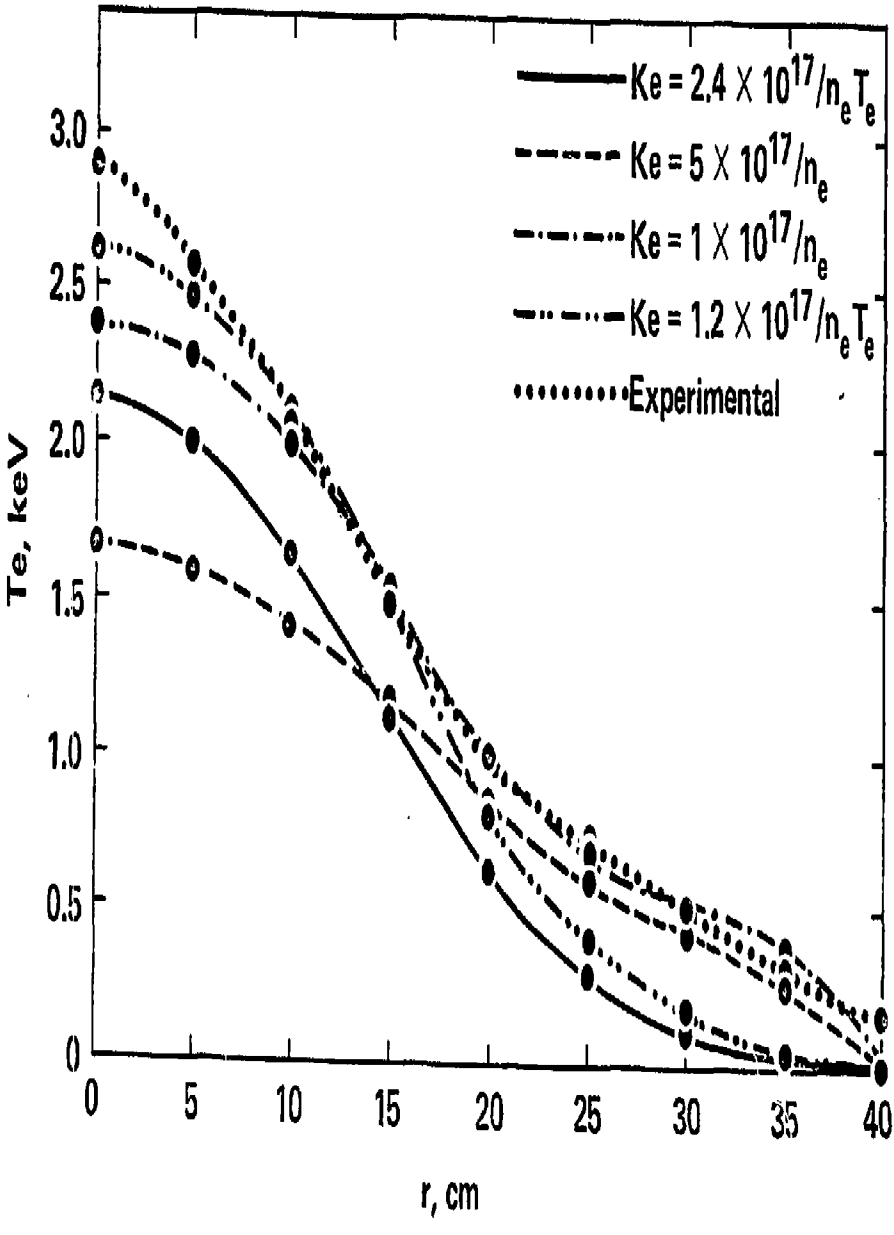

Fig. 6 Electron temperature profile vs. transpo model for PLT run number 88214.